

The ground state energy of the Edwards-Anderson spin glass model with a parallel tempering Monte Carlo algorithm

F Romá^{1,2}, S Risau-Gusman¹, A J Ramirez-Pastor², F Nieto²
and E E Vogel³

¹ Centro Atómico Bariloche, San Carlos de Bariloche, Río Negro R8402AGP ,
Argentina

²Departamento de Física, Instituto de Física Aplicada, Universidad Nacional de San
Luis - CONICET, Chacabuco 917, San Luis D5700BWS, Argentina

³Departamento de Física, Universidad de La Frontera, Casilla 54-D, Temuco, Chile

E-mail: froma@cab.cnea.gov.ar, srisau@cab.cnea.gov.ar,
antorami@unsl.edu.ar, fnieto@unsl.edu.ar and ee_vogel@ufro.cl

Abstract. We study the efficiency of parallel tempering Monte Carlo technique for calculating true ground states of the Edwards-Anderson spin glass model. Bimodal and Gaussian bond distributions were considered in two and three-dimensional lattices. By a systematic analysis, we have obtained the values of the appropriate simulation parameters for reaching quickly the ground state of large samples. The results establish that the performance of the parallel tempering technique is comparable to more powerful heuristics developed to find the ground state of Ising spin glass systems.

1. Introduction

The study of spin glasses is an active and controversial area of statistical physics. In particular, the properties of these systems at zero temperature have been intensively studied in the last years. The problem of finding ground states (GSs) is a very difficult subject because of quenched disorder and frustration that are present in most realistic spin glass models. In fact, it has even been shown that finding the GS of a spin glass in a three-dimensional lattice is an NP-complete problem [1], which means that this challenge is at least as difficult as the hardest known problems. As a consequence, many different algorithms have been proposed to solve it and to assess the efficiency of these algorithms is thus very important. *Genetic algorithms* [2] are considered as the most powerful heuristics to reach the GS of spin glass systems [3, 4]. After introduction of the triadic crossover by Pál [5, 6], different improvements have been made to combine genetic algorithms with, for example, *cluster-exact approximation* [7, 8] and *renormalization* [9]. Nevertheless, algorithms based in Monte Carlo (MC) methods, such as *simulated annealing* (SA) [10], *multicanonical ensemble* [11] and *parallel tempering* (PT) [12, 13], have also been used to find GSs of spin glasses. Just as genetic algorithms, they are simple to be implemented. However, MC methods are usually considered less efficient than genetic algorithms, because it is often assumed that the presence of a temperature parameter in the algorithm entails a breaking of the ergodicity that can lead to difficulties in the searching of GSs of disordered systems.

Recently, PT has been used to find the GS (see, for instance, [13, 14, 15]), and it has been shown [13] to be more efficient than other MC based algorithms. However, the issue of the efficiency of the PT algorithm has been very briefly discussed in the literature. In this work, we tackle this point in a more systematic way by analyzing how this efficiency depends on the different input parameters of the PT. The system to which the algorithm is applied is the Edwards-Anderson (EA) spin glass model [16] in two-dimensional (2D) and three-dimensional (3D) lattices, with both bimodal and Gaussian distributions of bonds. The results show that the performance of the PT technique is comparable to more powerful heuristics developed to find the GS of disordered and frustrated systems. Furthermore, we show that the efficiency depends of certain combinations of the parameters. In particular, we find a heuristic formula that gives the minimum time (in unit of time of PT algorithm, see below) that is necessary to find the GS with a fixed probability and for a given lattice size.

The paper is structured as follows. In section 2, we present the EA model and the PT method. In addition, different implementations of these algorithms are analyzed. In section 3, optimal parameters for 2D and 3D EA model with bimodal and Gaussian bond distributions are obtained for small lattice sizes. Then, the GS energy for larger sizes are calculated and the thermodynamic limit of this quantity is obtained. Conclusions are drawn in section 4.

2. Model and Algorithm

We consider the Edwards-Anderson spin glass model [16], which consists of a set of N Ising spins $\sigma_i = \pm 1$ placed in a square or cubic lattice of linear dimension L , with periodic boundary conditions in all directions. Its Hamiltonian is

$$H = \sum_{(i,j)} J_{ij} \sigma_i \sigma_j, \quad (1)$$

where (i, j) indicates a sum over nearest neighbors. The coupling constants or bonds, J_{ij} 's, are independent random variables drawn from a given distribution with mean zero and variance one. In this paper we concentrate on the EA model with two distributions: the bimodal (EAB), and the Gaussian (EAG). In the EAB case, the bonds take only two values $J_{ij} = \pm 1$, with equal probability. For relatively large system sizes, and due to the fact that the bonds are independent variables, only configurations with half of the bonds of each sign are statistically significant. To preserve this feature for small sizes, we explicitly enforce the constraint

$$\sum_{(i,j)} J_{ij} = \begin{cases} 0 & \text{for even number of bonds} \\ \pm 1 & \text{for odd number of bonds.} \end{cases} \quad (2)$$

For systems with an odd number of bonds, we enforce the constraint $\sum_{(i,j)} J_{ij} = 1$ for the half of the samples and $\sum_{(i,j)} J_{ij} = -1$ for the other half. In the EAG case, the bonds are drawn from a Gaussian distribution. One important difference between these models is that whereas for the EAG the GS of the system is unique (up to a global symmetry), the EAB has a highly degenerate GS.

In order to implement a PT algorithm [12] one needs to make m replicas of the system (ensemble) to be analyzed, each of which is characterized by a temperature parameter T_i ($T_1 \geq T_i \geq T_m$). The basic idea of this algorithm is to simulate independently a Hamiltonian dynamics (standard MC) for each replica, and to swap periodically the configurations of two randomly chosen temperatures. The purpose of this swap is to try to avoid that replicas at low temperatures get stuck in local minima. Thus, the highest temperature, T_1 , is set in the high-temperature phase where relaxation time is expected to be very short and there exists only one minimum in the free energy space. The lowest temperature, T_m , is set in the low-temperature phase. Within this interval we choose equally spaced temperatures, i.e. $T_i - T_{i+1} = (T_1 - T_m)/(m - 1)$.

As mentioned above, PT is based on two procedures that are performed alternately. In the first one, a standard MC method is used to independently simulate the dynamics of each replica: in each elementary step, the update of a randomly selected spin of the ensemble is attempted with a probability given by the Metropolis rule [17]. In the second procedure, a trial exchange of two configurations X_i and $X_{i'}$ (corresponding to the i -th and i' -th replicas) is attempted, and accepted with probability [12]

$$W(X_i, \beta_i | X_{i'}, \beta_{i'}) = \begin{cases} 1 & \text{for } \Delta \leq 0 \\ \exp(-\Delta) & \text{for } \Delta > 0, \end{cases} \quad (3)$$

where $\Delta = (\beta_{i'} - \beta_i) [H(X_i) - H(X_{i'})]$ and $\beta_i = 1/T_i$ (we have taken the Boltzmann's constant equal to one without loss of generality). As in Ref. [12], we restrict the replica exchange to the case $i' = i+1$. The unit of time in this process or PT step (PTS) consists of a fixed number of elementary steps of standard MC, followed by other fixed number of trials of replica exchange. The initial configuration of each replica is usually random but, as discussed below, other choices can endow the algorithm with some interesting features. The running time, t_{sec} (in seconds), of our code can be approximated by

$$t_{sec} = \alpha m n t N, \quad (4)$$

where t is the number of PTSs, n is the number of independent runs and α is a constant.

Depending on the way we combine the number of elementary steps of standard MC and the number of replica exchanges, we define three different variants of the PT algorithm. The one that we call A algorithm consists of two stages. The first is simply a SA routine implemented as follows. Starting from a random initial condition, $t_A/2$ MC steps (MCSs) of standard MC are applied to replica 1 (each MCS consists of N elementary steps of standard MC). Next, the same is done successively for each replica, but taking the last configuration of replica i as the initial condition of replica $i+1$. The final configurations obtained according the procedure described previously are used to initialize a PT algorithm. In the second stage, we define that a PTS consists of $m \times N$ cycles, each cycle being one elementary step of standard MC plus one replica exchange. After $t_A/2$ PTSs, the algorithm stops and its output is the configuration with the smallest energy among all configurations visited by all replicas in the simulation process.

In the second variant, that we call B, the m replicas are initialized with a random configuration and the PTS consists of $m \times N$ elementary steps of standard MC and only one replica exchange. This definition is usually chosen to reach equilibrium. After t_B PTSs the algorithm stops and the configuration with lowest energy is stored.

Finally, a third variant, called C, consists only of the second stage of variant A, but with the initial configurations randomly chosen. After t_C PTSs (where the PTS is defined as in A algorithm), the configuration with minimum energy is stored.

To compare the performance of the three variants proposed, we run each one of them on the same $N_S = 10^3$ samples of the 2D EAB model (only one run for sample). We choose the values of parameters t_A , t_B and t_C in such a way as to ensure that the running time of the three variants is the same. In our case, we have used $t_A = 2t$, $t_B = 2.3t$ and $t_C = 1.5t$ (this choice depends on the particular implementation of each algorithm). In order to check whether the final configuration found by each algorithm is really a ground state, we compare with the output of an exact branch-and-cut algorithm run on the same sample [18, 19]. The quantity we choose to compare the efficiency of the variants A, B and C is the mean probability of finding the GS, \mathcal{P}_0 , which we estimate as

$$P_0 = \frac{1}{N_S} \sum_{j=1}^{N_S} P_{0,j}, \quad (5)$$

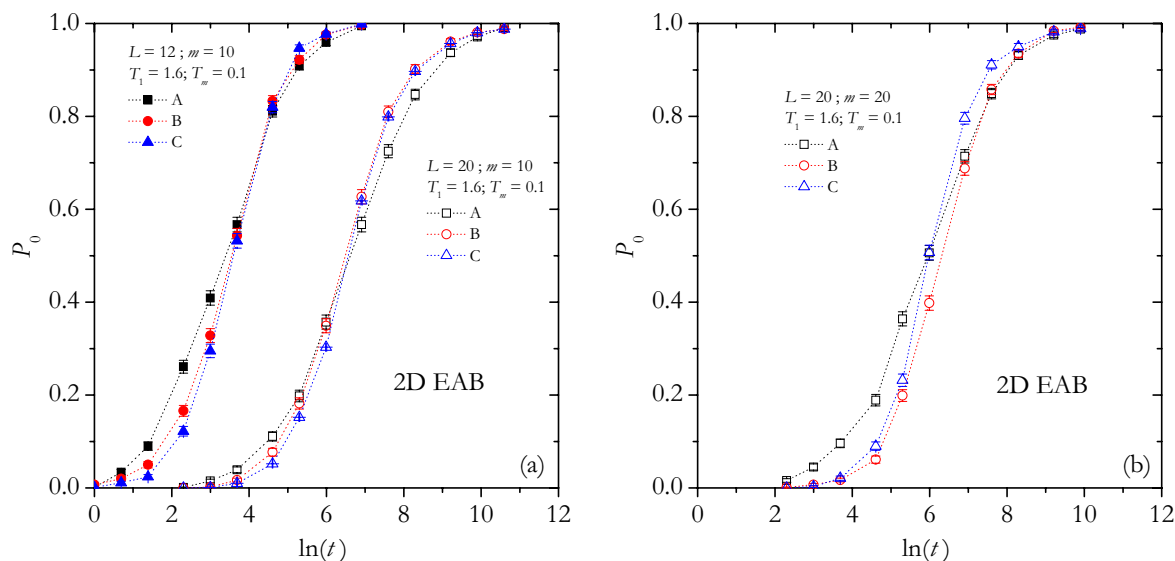


Figure 1. P_0 as function of $\ln(t)$ for the 2D EAB model, calculated with three variants of the PT algorithm. In all cases, the range of temperatures used varies between $T_1 = 1.6$ and $T_m = 0.1$. (a) $L = 12$ and $L = 20$ with $m = 10$, and (b) $L = 20$ with $m = 20$.

where

$$P_{0,j} = \frac{n_j}{n}, \quad (6)$$

is an estimation of the probability of reaching the GS for the j -th sample, $\mathcal{P}_{0,j}$. In the last equation n_j is the number of times that GS is found for the j -th sample in n independent runs. Note that in this example we use $n = 1$. Therefore for each sample $P_{0,j} = 0$ or 1 . As it is shown in the appendix A, the error associated to P_0 becomes small if many samples are considered and only one run is carried out in each one of them (it is not necessary to consider many runs for sample, i.e. $n \gg 1$).

The result of this comparison is shown in figure 1 for different values of L and m (see appendix A for a detailed calculation of the error bars). It can be seen that the performance of the three variants is very similar for all values of t . However, an exhaustive analysis shows that for $P_0 > 0.5$, the performance of B and C algorithms is a little better than the one corresponding to A and this behavior is reinforced upon increasing the lattice size [see figure 1 (a)]. On the other hand, by comparing the curves for $L = 20$ in figures 1 (a) and (b), we observe that if m is increased, the probability P_0 for A and B are the same, while for C is a little larger. These examples show that the PT algorithm has a complex dependence with m . The above comparison has been performed also for the other studied cases (2D EAG, 3D EAB and 3D EAG models) and the results are very similar to those shown in figure 1. The most important feature is that in the large P_0 regime, the performance of A is always worse than the other two, which means that its performance could be used as a lower bound for the B and C cases. This line of reasoning leads to focus on analyzing the performance of A only. In addition, we show below that variant A presents very interesting scaling properties. To

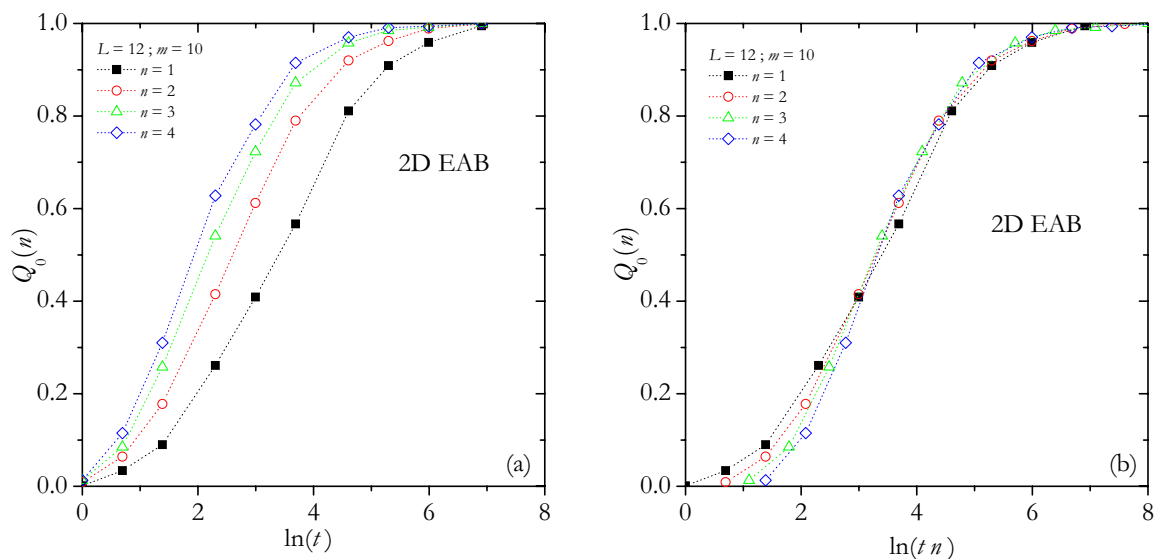


Figure 2. $Q_0(n)$ for the 2D EAB model with $L = 12$, $m = 10$ and different values of n as indicated. (a) $Q_0(n)$ vs. $\ln(t)$, and (b) $Q_0(n)$ vs. $\ln(t n)$.

avoid confusions, we keep $t_A = 2t$ in the rest of this paper.

3. Results

In this section we study the A algorithm for the EAB and EAG models in 2D and 3D. The first issue we address is whether it is better to use a large t and one run for each sample, or in turn, several runs but with a smaller t . The quantity to be studied for this purpose is $Q_0(n)$, which is the sample average of the probability that a GS is found in at least one of the n independent runs in the j -th sample, $Q_{0,j}(n)$. Figure 2 (a) shows the estimate of this quantity, $Q_0(n)$, as a function of $\ln(t)$ for $n = 1, 2, 3$ and 4 . We use $N_S = 10^3$ samples of $L = 12$ and $m = 10$. As expected, the performance improves with increasing n . However, when time is rescaled to $\ln(t n)$ in order to compare the performances at the same running time (see Eq. 4), independently of the number of runs, the curves approximately collapse [see figure 2 (b)]. Then, the performances are similar for all values of n when the total running time is considered, especially in the high Q_0 region. As this is a recurrent feature in all tested cases, in the rest of this article we concentrate in the case $n = 1$.

In the following, the plan is first to determine the range of temperatures which is *globally optimal*. Although for each particular problem (EAB or EAG in either 2D or 3D) is possible to determine an optimal set, for practical purpose we have chosen to fix the range of temperatures. Then, we will focus on the number of replicas and the time t . Finally, the analysis for small size will allows us to predict the optimal values of these parameters for larger lattice sizes.

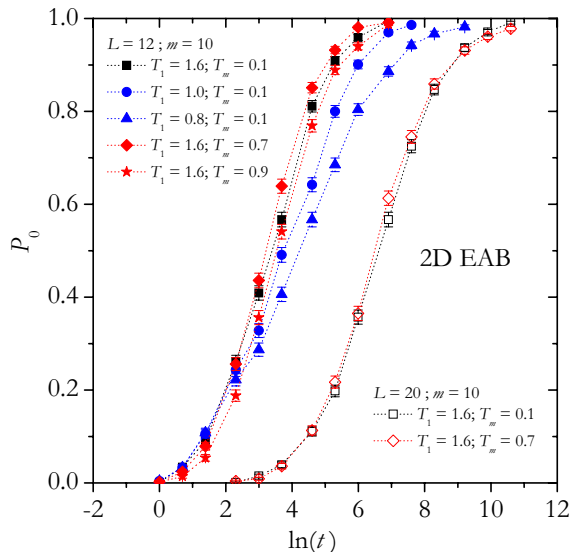


Figure 3. P_0 as function of $\ln(t)$ for the 2D EAB model with $L = 12$ and $L = 20$. The curves correspond to different ranges of temperatures as indicated.

3.1. 2D EA models

We begin by discussing the criteria for selecting the more appropriate range of temperature for each studied system. As mentioned above, it is important that the highest temperature T_1 is set in the high-temperature phase: $T_1 > T_c$, where T_c is the critical temperature. Although for the 2D EA models $T_c = 0$, below $T \approx 1.3$ the dynamics is slow [20] and the system has very long relaxation times. Then, it is reasonable to expect that the optimal T_1 should be $T_1 > 1.3$. On the other hand, as the algorithm is designed to reach the GS, the lowest temperature T_m should be very low (but not zero because the Metropolis rule is not efficient in that case).

As in the previous section, we run the algorithm with several different temperature ranges, on $N_S = 10^3$ different samples per size (in the following, this number of samples is used for all 2D calculations). P_0 for the EAB model is shown in figure 3. We find that, if we fix the lowest temperature at $T_m = 0.1$, for the case $L = 12$, the highest temperature should not be lower than $T_1 = 1.3$. On the other hand, if we choose the highest temperature at $T_1 = 1.6$, the lowest temperature should not be higher than $T_m = 0.7$. However, as seen for $L = 20$, both ranges $T_1 = 1.6$ to $T_m = 0.1$ and $T_1 = 1.6$ to $T_m = 0.7$, give similar results. The conclusion is that the performance of the algorithm depends only weakly on the range of temperatures chosen under the condition that a) the largest temperature is outside the region of slow dynamics ($T_1 > 1.3$) and b) the lowest temperature is not too high (say, $T_m < 0.7$). This conclusion is also valid for the EAG model. Therefore, in the remaining of this subsection we use $T_1 = 1.6$ and $T_m = 0.1$ for all the simulations.

We now discuss the dependence of probability P_0 on parameters L , m and t . Figure 4 (a) shows the curves of probability for different lattice sizes and number of

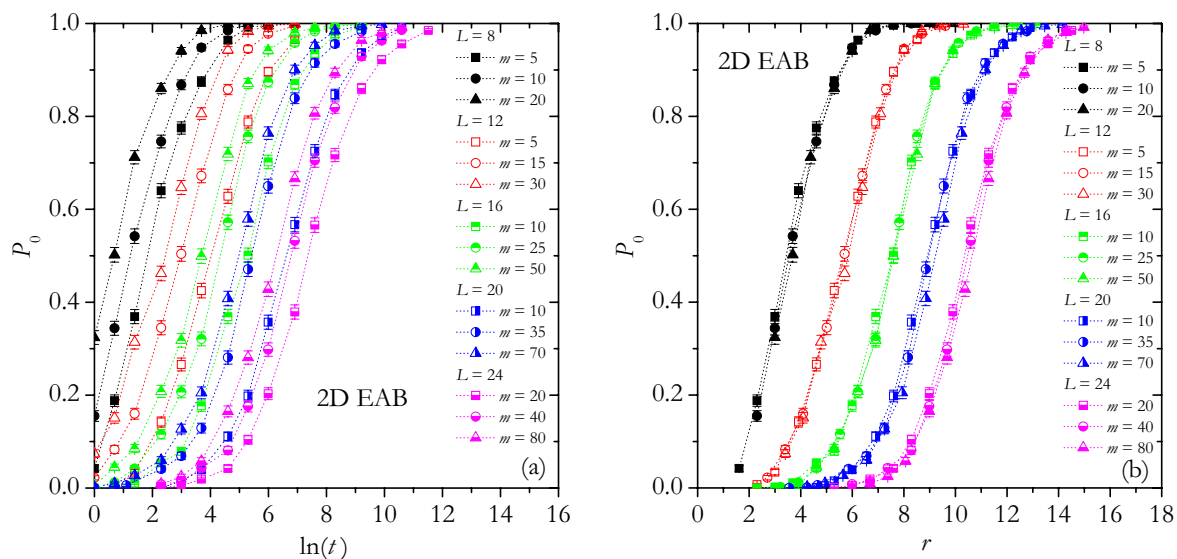


Figure 4. P_0 as function of (a) $\ln(t)$ and (b) r for the 2D EAB model. The curves correspond to different lattice sizes and number of replicas as indicated.

replicas. As was to be expected, for fixed values of t , P_0 increases with m . Thus, given that the running time is proportional to $t m$ (see Eq. 4), is reasonable to draw the curves as functions of

$$r \equiv \ln(t m), \quad (7)$$

as in figure 4 (b). Interestingly, the curves for different m and fixed L collapse to the same curve. This non-trivial behavior shows that, approximately, P_0 is a function of r for fixed size ‡.

We now turn to the L dependence of the curves shown in figure 4 (b), with the hope that they too can be collapsed onto a single curve. First, note that the inflection point is located approximately at $P_0 = 0.5$. Figure 5 (a) shows that r_0 , the value of r at $P_0 = 0.5$, is a linear function of $L^{1/2}$. By fitting these points with the function

$$r_0 = bL^c - a, \quad (8)$$

we obtain $b = 3.35(7)$ and $a = 5.86(28)$ (c is fixed to $c = 1/2$, but it is left as a variable in the equation because its value is different in 3D). This leads us to rescale the abscissa axis of figure 4 (b), using the variable

$$x = [r - (bL^c - a)]/L^d. \quad (9)$$

Figure 5 (b) shows that, for $d = 0.2$, this rescaling collapses all the curves of figure 4 (a) onto a single curve.

Even though the rescaling proposed is not rigorous, it allows us to predict the value of r for each lattice size L and for a given probability P_0 with great accuracy.

‡ For the B algorithm this striking property does not hold.

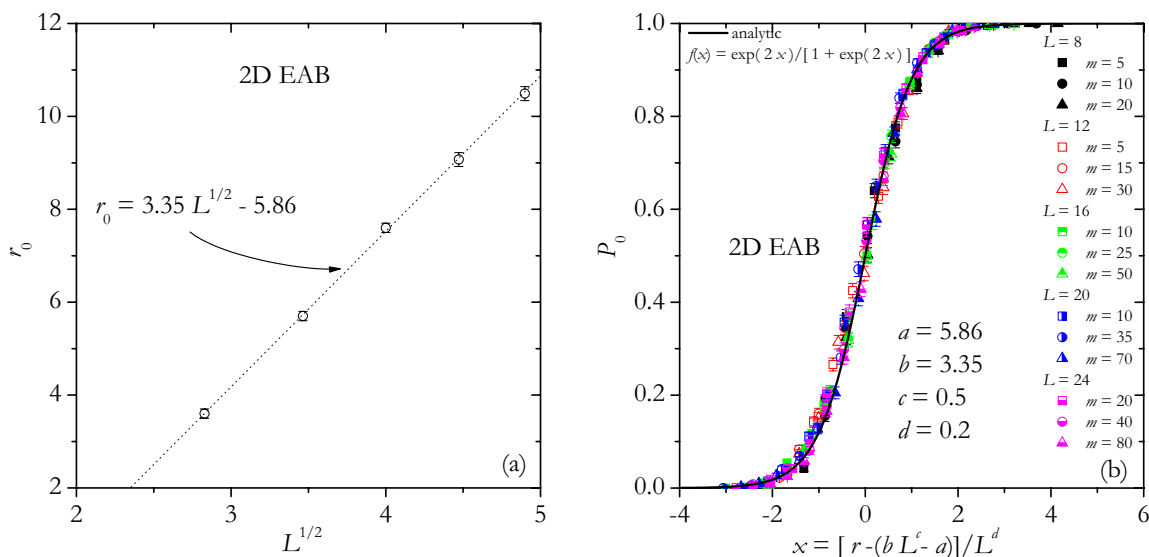


Figure 5. (a) r_0 vs. $L^{1/2}$ for the 2D EAB model. (b) Data collapsing for all curves in figure 4 (a).

Furthermore, all data points of figure 5 (b) can be fitted by the function

$$f(x) = \frac{\exp(qx)}{1 + \exp(qx)}, \quad (10)$$

where $q = 2$ [see figure 5 (b)]. By combining Eqs. (9) and (10), we can obtain a simple expression to predict the number of PTSs necessary to reach the GS with a given value of P_0 ,

$$t = \frac{1}{m} \left(\frac{P_0}{1 - P_0} \right)^{\frac{L^d}{q}} \exp(bL^c - a). \quad (11)$$

Now, we repeat the previous analysis for the EAG model. Figures 6 (a) and (b) show the probability P_0 for different lattice sizes and number of replicas as functions of $\ln(t)$ and r , respectively. Even though the collapse in this case is not as good as for the EAB model, it is still very good in the region of high P_0 ($P_0 \gtrsim 0.9$). Figure 7 (a) shows r_0 as function of $L^{1/2}$. As before, we fit these points with Eq. (8) and we obtain $b = 4.61(14)$ and $a = 6.34(46)$ ($c = 1/2$). Next, a second collapsing of the data is shown in figure 7 (b), again for $d = 0.2$. This collapse is very well fitted by the function in Eq. (10) with $q = 2$ [see figure 7 (b)].

One difference with the EAB case is that the value of the parameter b is larger, which implies that, for example, for $L = 20$, $m = 10$ and $P_0 \approx 0.99$, the required number of PTSs for the EAG model is two orders of magnitude larger than for the EAB model. This is also a common feature of other heuristics as genetic algorithm, where GSs are harder to obtain for Gaussian than for bimodal bond distributions. The reason is that the GS of the EAG model is unique, while it is degenerate for the EAB model, making it easier to find because any one of them is sufficient [21]. In fact, the ground-state

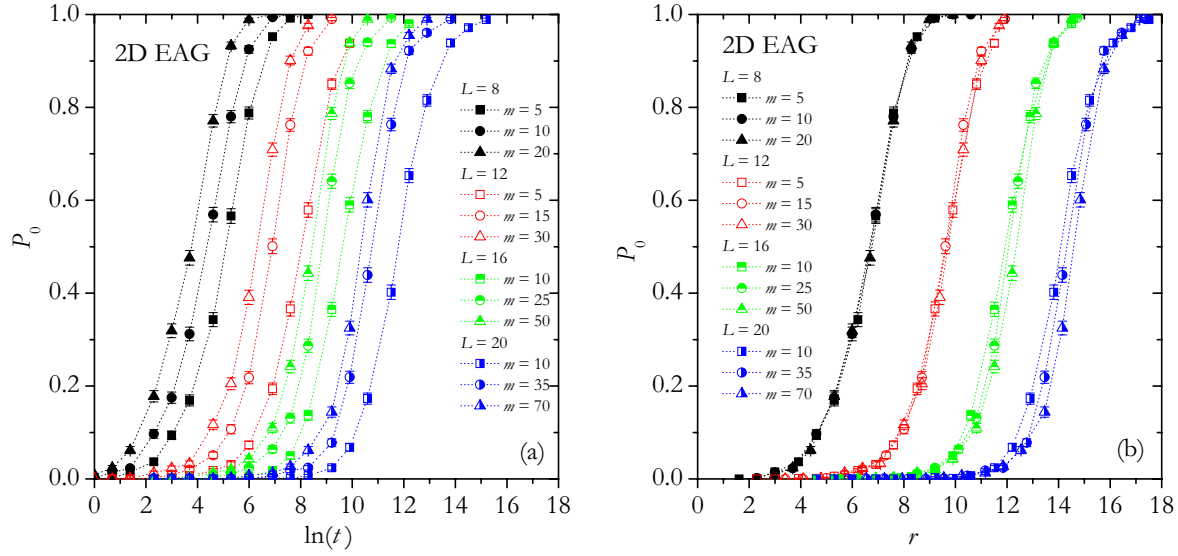


Figure 6. P_0 as function of (a) $\ln(t)$ and (b) r for the 2D EAG model. The curves correspond to different lattice sizes and number of replicas as indicated.

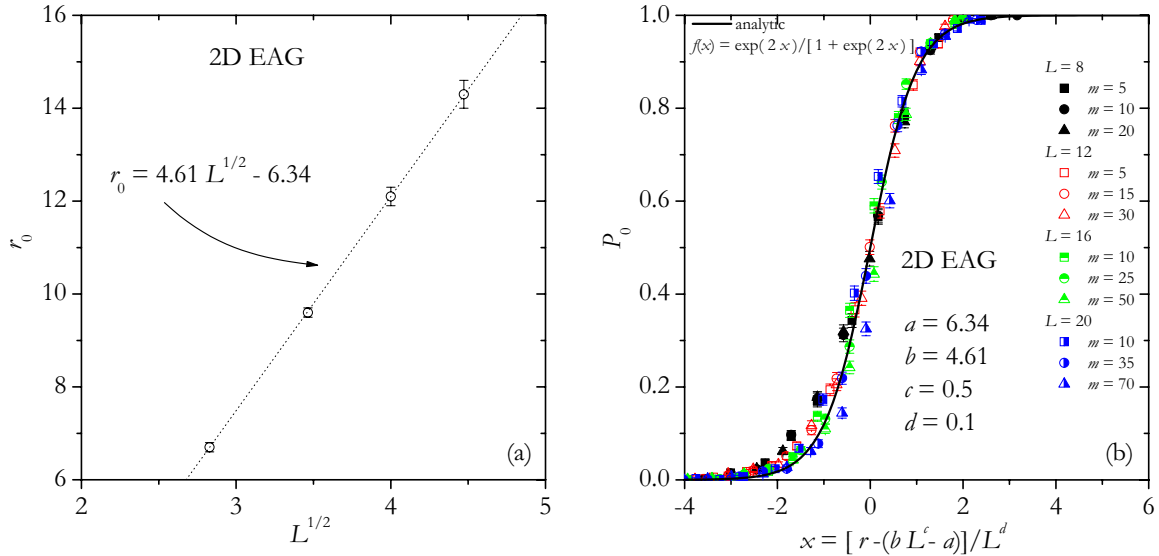


Figure 7. (a) r_0 vs. $L^{1/2}$ for the 2D EAG model. (b) Data collapsing for all curves in figure 6 (a).

entropy per spin for the EAB model with $L = 20$ is approximately $S = 0.0818$ [22], what implies that the number of GSs is $\sim 1.6 \times 10^{14}$.

3.2. 3D EA models

In the previous analysis for 2D lattices we have checked the GS energies obtained by PT, comparing them with the exact ones calculated with branch-and-cut algorithm [18]. But finding the GS of a 3D system is a much more difficult task, and exact algorithms available to us can only be used for small lattices (up to $L = 6$). Therefore, a different

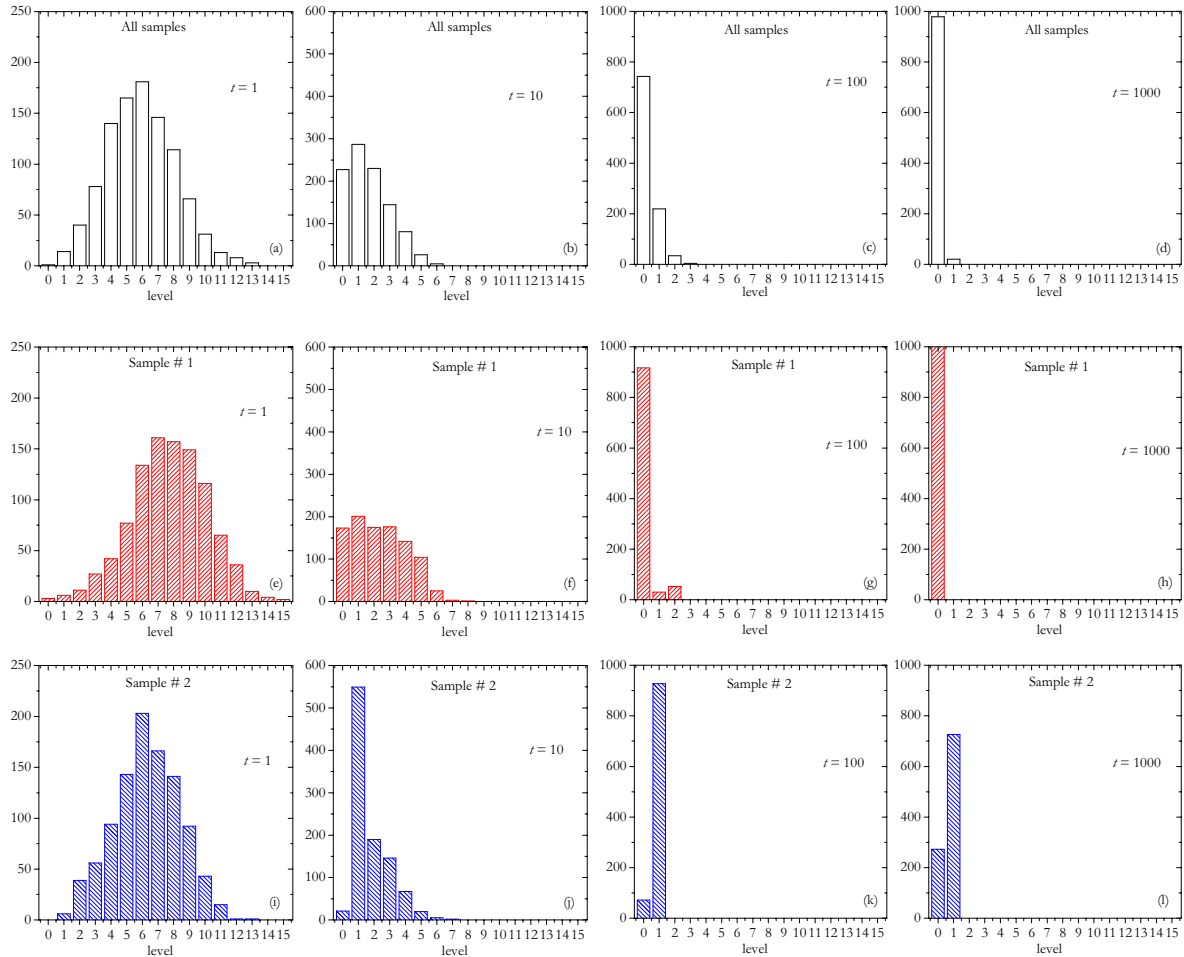


Figure 8. Energy levels found for the PT algorithm for the 3D EAB model with $L = 6$, $m = 20$ and times $t = 1, 10, 10^2$ and 10^3 . Histograms for (a)-(d) $N_S = 10^3$ different samples, (e)-(h) an easy sample (#1) and (i)-(l) a hard sample (#2).

strategy must be used to ensure that the configurations found by our algorithm really correspond to true GSs. The method we have used is as follows. First, we run the algorithm for a certain time t , for each sample of a given set. Then, the algorithm is run anew but now duplicating the time t . This is repeated many times, and thus a series of configurations, with their energies, are stored. We stop this process when, for each sample, in two successive runs the same minimum energy is obtained §. Comparing the series of energies, we can separate them into "easy" and "hard" samples (the GS energy of an easy sample is obtained in a few steps of the previous process, while for a hard sample many more steps are necessary). In this stage, we assume that the true GS has been found for all easy samples. On the other hand, for hard samples the previous process is continued and it is assumed that the true GS has been found when in three successive runs the same energy is obtained. We used these energies to calculate the

§ Note that the process continues in all samples, while at least the minimum energy for one sample changes in two successive runs

probability P_0 for all 3D samples studied in this subsection. Note that the number of PTSs used for reaching the GS is not necessarily optimal, i.e. it is not impossible that the GS can be found in shorter times.

In Figure 8 we can see the difference between the histogram (number of samples) of the energy levels obtained with the PT algorithm for many samples, and the ones obtained by performing many independent runs of the algorithm on both, an easy and a hard sample. Figures 8 (a)-(d) show the histograms for $N_S = 10^3$ samples of the 3D EAB model with $L = 6$, $m = 20$ and four different numbers of PTSs: $t = 1, 10, 10^2$ and 10^3 (one run for each sample). As it can be observed, for short times such as $t = 1$ and $t = 10$, the histogram is broad and the maximum is not located in the ground level. For long t , the shape of the histogram changes and a peak arises at the ground level. In fact, as $t = 10^3$ is used, the GS energy is found in 979 samples (the remaining 21 are located in the first excited level).

A similar behavior is observed for the easy sample (#1), figures 8 (e)-(h). In this case, instead of many samples, one sample and $n = 10^3$ independent run are used. For $t = 10^3$, the PT algorithm always finds a true GS. On the other hand, as it is shown in figures 8 (i)-(l), a different behavior is observed for the hard sample (#2). For all t , the peak is not located at the ground level. Thus, for $t = 10^3$ the true GS is found in only 273 of the runs. This example shows that the properties of hard samples are not reflected in the global behavior [figures 8 (a)-(d)] and justifies our previous protocol to obtain true GS in these samples.

In order to study the influence of the temperature range on the performance of our algorithm, it is important to bear in mind that for 3D $T_c > 0$. For practical purposes, we can consider that $T_c \approx 1.12$ for the EAB model and $T_c \approx 0.95$ for the EAG model [23]. After a similar analysis to the one carried out above for 2D models, we conclude that $T_1 = 1.6$ and $T_m = 0.1$ are the adequate limits for the 3D case and they will be used throughout the section.

Now, we run the PT algorithm for the EAB model with $L = 4, 6, 8$ ($N_S = 10^3$ for each size) and $L = 10$ ($N_S = 10^2$). In all cases, we set $n = 1$. Figures 9 (a) and (b) show the mean probability P_0 vs $\ln(t)$ and r , respectively. The collapse obtained is very good, as for the 2D EAB model. As shown in figure 10 (a), r_0 is now a linear function of L with $b = 1.36(4)$ and $a = 1.57(33)$. If the data are rescaled using x , a very good collapse is obtained, as shown in figure 10 (b) for $c = 1$ and $d = 1$ (in the linear fit and data collapsing were only considered lattice sizes $L = 6, 8$ and 10). As before, Eq. (11) gives a very nice fit of all these data points, but now with $q = 6.5$.

Unfortunately, when the same analysis is carried out for the EAG model the results are not so good. Figures 11 (a) and (b) show that the collapse of the curves as function of r is not as good as for the 3D EAB case (even in the high P_0 region). Here, the parameters used were $N_S = 10^3$ samples for each size $L = 4, 5, 6, 7$ and 8 . Figure 12 (a) shows the dependence of r_0 with L . Using the same fitting function, we obtain $b = 1.67(7)$ and $a = 0.66(43)$ (only lattice sizes with $L > 4$ were considered). The collapse of the data obtained with these values is not very good, we have preferred to

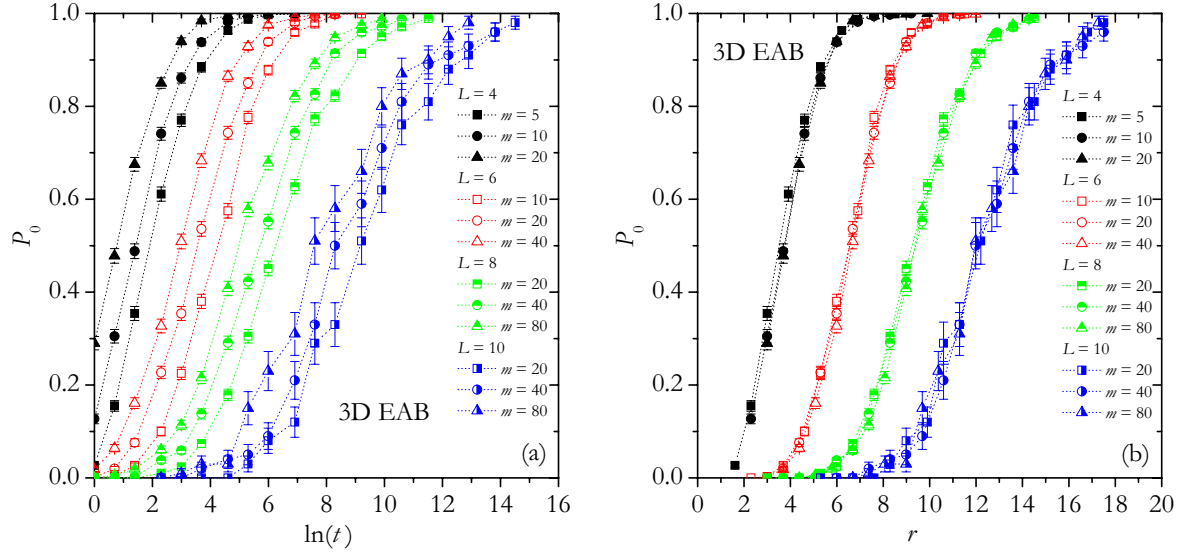


Figure 9. P_0 as function of (a) $\ln(t)$ and (b) r for the 3D EAB model. The curves correspond to different lattice sizes and number of replicas as indicated.

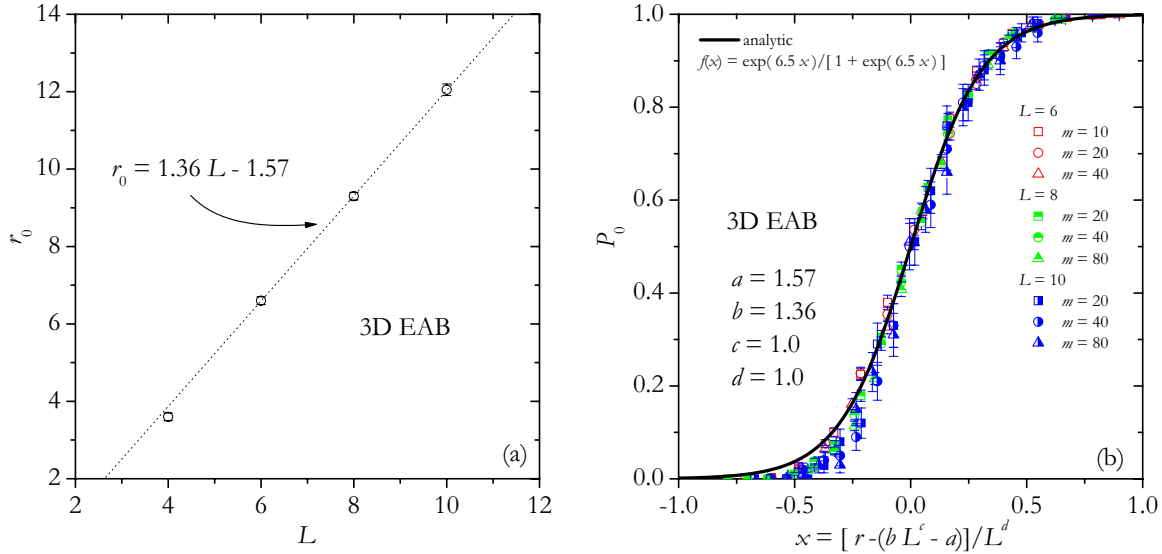


Figure 10. a) r_0 vs. L for the 3D EAB model. (b) Data collapsing for all curves in figure 9 (a).

fit the data for only one value of m ($m = 20$). Figure 12 (a) shows the dependence of r_0^* (r_0^* is the value of r at $P_0 = 0.5$ and $m = 20$) on L , where the fit for $L > 4$ gives $b = 1.55(3)$ and $a = -0.05(20)$. Data collapsing in figure 12 (b) has been obtained with these parameters, $c = 1$ and $d = 0.2$. The function Eq. (11) with $q = 2$ gives a very good fit for $m = 20$, and a reasonable good fit for all the other points. If small lattice sizes are discarded ($L = 4$ and 5), we obtain a good collapse for $b = 1.50(2)$, $a = -0.43(11)$, $c = 1$, $d = 1$ and $q = 10$, (these parameters are similar to the corresponding ones in the 3D bimodal case).

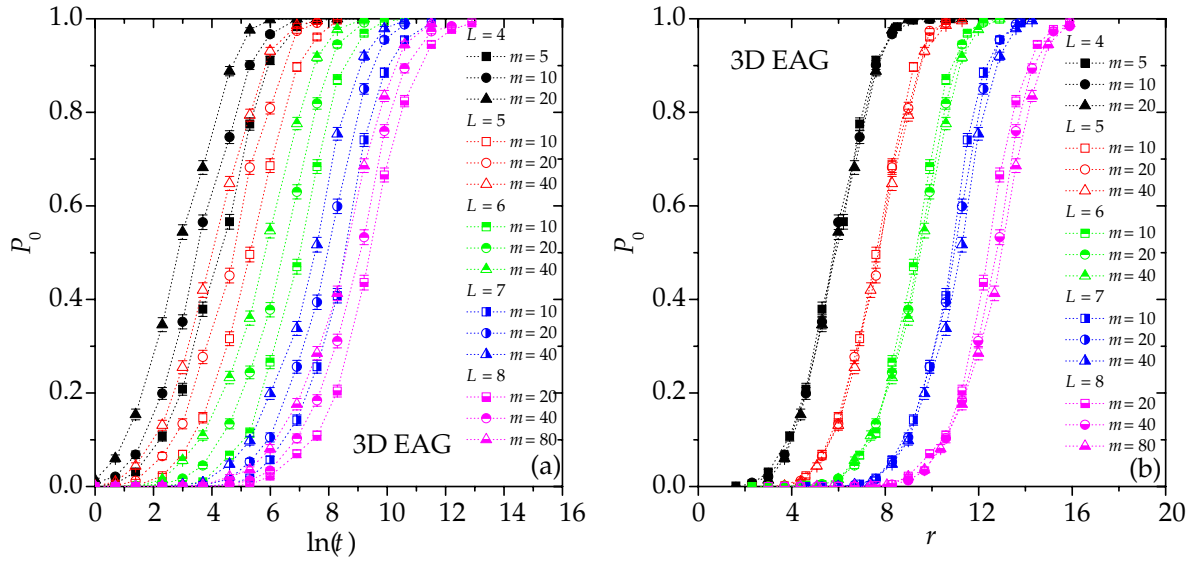


Figure 11. P_0 as function of (a) $\ln(t)$ and (b) r for the 3D EAG model. The curves correspond to different lattice sizes and number of replicas as indicated.

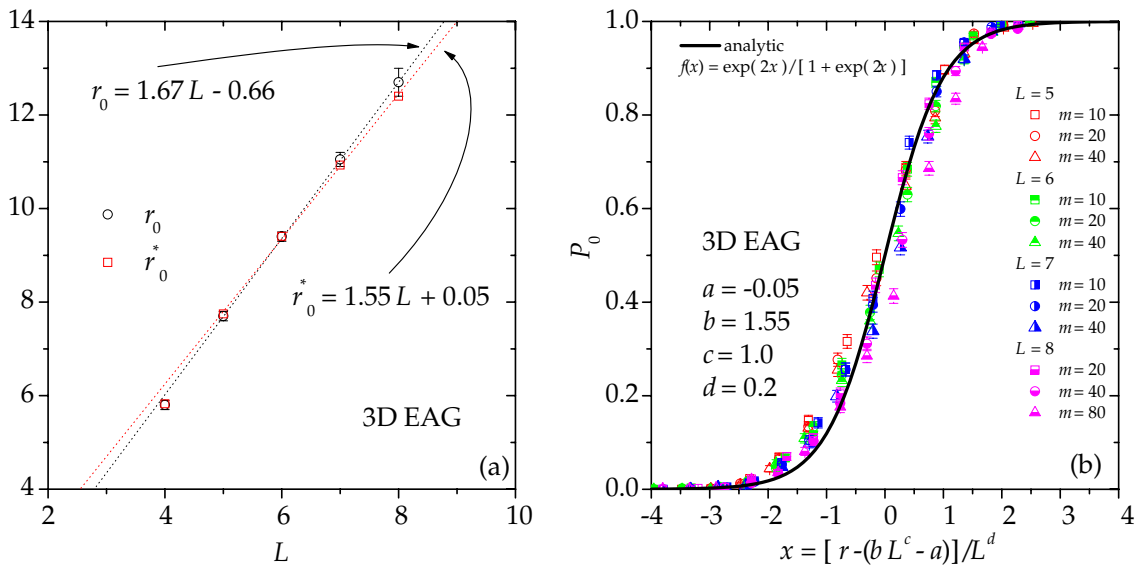


Figure 12. a) r_0 and r_0^* vs. L for the 3D EAG model. (b) Data collapsing for all curves in figure 11 (a).

Finally, to show the importance of the replica exchange procedure, we compare the performances of the PT and the SA algorithms. In figures 13 (a) and (b), we show results for the 3D EAB model with $L = 8$. To carry out an appropriate comparison, we implement the SA as the first stage of our PT algorithm A, but now we define t_{SA} as the number of MCSs used in each temperature. By choosing $t_{SA} = 4t$, we ensure that both algorithms have the same running time. It is evident that the performance of the PT algorithm is superior and only for short t the SA method is more efficient.

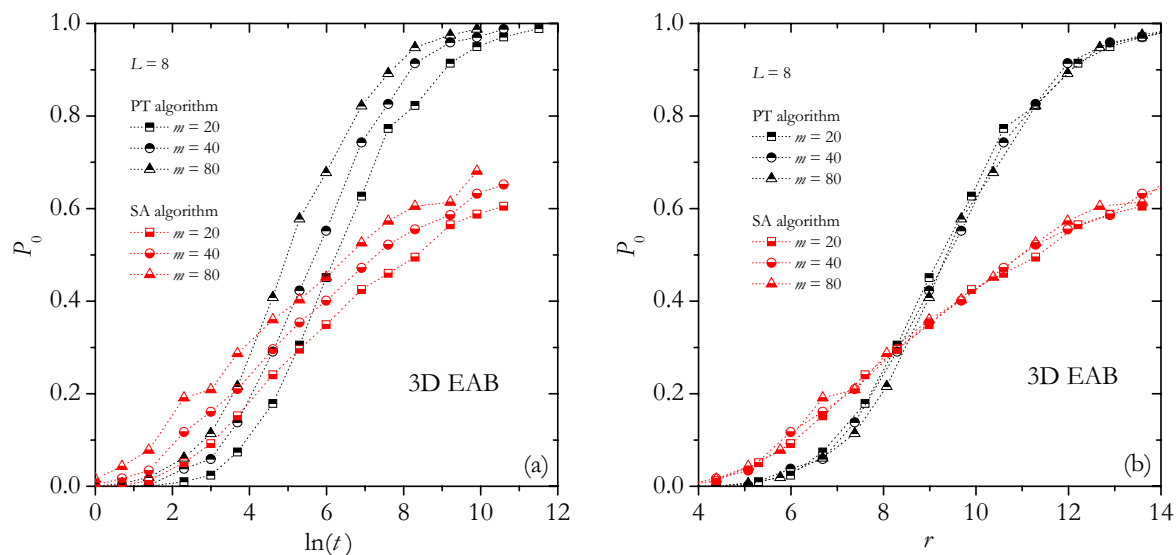


Figure 13. Comparison between the PT and SA algorithms for the 3D EAB model with $L = 8$. Figures show the probability P_0 as function of (a) $\ln(t)$ and (b) r .

Table 1. Parameters defined in Eqs. (4), (11) and (12) for the different studied models.

Model	a	b	c	d	q	α	u_∞	g	e
2D EAB	5.86	3.35	0.5	0.2	2.0	1.1×10^{-7}	-1.4019(8)	1.40(8)	2.02(5)
2D EAG	6.34	4.61	0.5	0.2	2.0	2.1×10^{-7}	-1.3147(4)	1.39(7)	2.33(4)
3D EAB	1.57	1.36	1.0	1.0	6.5	1.4×10^{-7}	-1.7867(2)	2.89(6)	2.93(2)
3D EAG	-0.05	1.55	1.0	0.2	2.0	2.7×10^{-7}	-1.7000(3)	2.01(8)	2.94(4)

3.3. Ground state energy

We performed the calculation of the GS energy per spin, u_L , for larger 2D and 3D lattices. In all cases, we choose $m = 20$ and as before, $n = 1$, $T_1 = 1.6$ and $T_m = 0.1$. Next, we use the Eq. (11) with the parameters given in table 1 and a given probability P_0 , to predict the number of PTSs needed. All calculations were carried out using a computer cluster of 40 PCs each with a 3.0 GHz Dual Intel(R) Xeon(TM) processor \parallel . The running time t_s (in seconds) it can be calculated with Eq. (4) and the value of α given in table 1.

Tables in appendix B show, for each studied model, the value of the GS energy per spin obtained with the PT algorithm and the parameters used in the simulation: namely the number of samples and the number of PTSs (calculated with Eq. (11)). With these quantities, the GS is found with an approximate probability P_0 (which is also shown in tables of appendix B). Figures 14 (a) and (b) show the results for the GS energy per spin. By fitting these data points with the function

$$u_L = u_\infty + gL^{-e}, \quad (12)$$

\parallel Computer cluster of the Comisión Nacional de Energía Atómica, Centro Atómico Bariloche, Argentina.

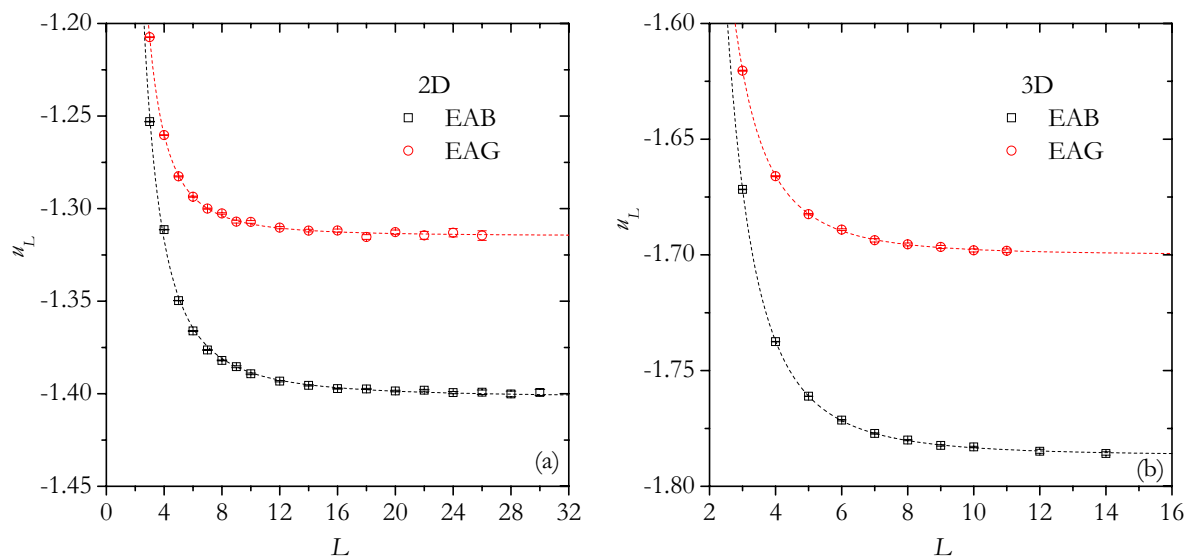


Figure 14. GS energy per spin for the EAB and EAG models in (a) 2D and (b) 3D.

we obtain u_∞ , the GS energy in the thermodynamic limit. The values of these energies and the remaining parameters (g and e) are given in table 1.

The most accurate values of the GS energy in the thermodynamic limit reported in the literature are: 2D EAB $u_\infty = -1.40193(2)$ [24], 2D EAG $u_\infty = -1.31479(2)$ [25], 3D EAB $u_\infty = -1.7863(4)$ [6] and $u_\infty = -1.7876(3)$ [8], and 3D EAG $u_\infty = -1.7003(8)$ [21]. The values calculated in this work agree within the error bars with these. In addition, the GS energy for *each lattice size* in 3D (tables B3 and B4), agrees within the error bars with the values reported previously in the literature for the EAB [6, 8, 26] and EAG [21, 28] models.

4. Conclusions

In this work we have used a PT algorithm to find the GS energy of the EA model with both bimodal and Gaussian bond distributions. In general, this heuristic can be easily implemented to solve a very general class of problems: systems with any boundary conditions, with arbitrary forms of interactions, with or without external field, with any dimensionality, etc. This is the most important feature of the PT algorithm. We have checked that, for large lattice sizes, the A variant of our algorithm is always a lower bound of the performance of variants B and C in the high P_0 regime ($P_0 > 0.9$). For practical purposes, Eq. (11) with the parameters given in table 1 can be used to calculate the number of PTSs for the three variants (with $t_A = 2t$, $t_B = 2.3t$ and $t_C = 1.5t$). For a given t , the error in the probability P_0 predicted by Eq. (11) is not larger than 1%.

The performance of PT is comparable to the performance of more powerful heuristics, developed exclusively to find the GS of Ising spin glass systems. In 2D, this algorithm allows us to study systems with lattice sizes up to approximately $L = 30$ and $L = 26$ for, respectively, EAB and EAG models with fully periodic boundary

conditions. Although larger sizes can be analyzed by using matching algorithms [3], this can only be done for planar lattices (i.e. lattices with at least one free boundary condition). But, for such lattices, it has been found that very large system sizes must be used to have a reliable estimate of the thermodynamic limit of the GS energy (and other quantities), which somewhat undermines the advantages of having a faster algorithm. For lattices with fully periodic conditions, on the other hand, it has been shown that the energy converges to the thermodynamic limit for relatively small system sizes. For these systems, the branch-and-cut algorithm [18] is the fastest exact algorithm to calculate GSs of the EA model. Unfortunately, its implementation is rather difficult. As far as we know, the most efficient implementation of this heuristic is available on the server at the University of Cologne [19].

Contrary to the 2D case, finding the GS of a spin glass in a 3D lattice is a very difficult task, which has even been shown to be NP- complete [1]. Although an exact branch-and-cut algorithm has been developed for the EAG model, it can only find GSs of samples up to $L = 12$ with free boundary conditions [27, 29]. Thus, 3D systems with fully periodic boundary conditions constitute the most important application of heuristic algorithms. Among these, genetic search methods are usually considered as the most powerful techniques to find the GS of spin glass systems. Nevertheless, in this work we have shown that, for the same task, a simple PT algorithm performs as well as the genetic methods reported in the literature (i.e. similar systems sizes can be analyzed with the same computational effort). For example, for the 3D EAB model it has been reported that a genetic algorithm needs on average 392 minutes on a computer with a 134MHz R4600 processor [6], or 540 minutes on a computer with a 80MHz PPC601 processor [8], to perform a run in samples of $L = 14$. In Ref. [8], 100 samples of this size were calculated and 40 independent runs for each sample were carried out. On average, in only 13.8 of these runs the minimum energy was obtained [8]. Thus, we deduce that the GS was found with $P_0 \approx 13.8/40 = 0.345$. For this same probability, our algorithm requires approximately 60 minutes on a computer with a 3.0 GHz Dual Intel(R) Xeon(TM) processor. Although a direct comparison between these results is inappropriate (because these works were carried out more than ten years ago), probably the performances of both heuristics are comparable.

Finally, we consider the Ref. [21] where samples of size up to $L = 10$ for the 3D EAG model were calculated with $P_0 \approx 0.9$, by using a genetic algorithm with local optimization. With the PT algorithm, we have obtained similar results for $L = 10$, and for $L = 11$ we have found the GS with $P_0 \approx 0.8$. On the other hand, for the same model recently a genetic renormalization algorithm has been introduced, which is able to solve lattices up to $L = 12$ [4, 9]. Unfortunately, we have not been able to compare our results with those obtained by using this fast algorithm, because in Ref.[9] the energies for each lattice size have not been reported.

Acknowledgments

FR and EEV thank Millennium Scientific Initiative (Chile) under contract P-02-054-F for partial support. FR, FN and AJRP thank Univ. Nac. de San Luis (Argentina) under project 322000. We acknowledge support from CONICET (Argentina) under project PIP6294 and FONDECYT (Chile) under projects 1060317 and 7060300.

Appendix A. Error bars

The mean probability of reaching the GS is

$$\mathcal{P}_0 \equiv \langle P_{0,j} \rangle. \quad (\text{A.1})$$

In order to estimate \mathcal{P}_0 , we use Eqs. (5) and (6),

$$P_0 = \frac{1}{N_S} \sum_{j=1}^{N_S} \frac{n_j}{n}. \quad (\text{A.2})$$

In the last equation we have estimate the probability of reaching the GS for the j -th sample, $\mathcal{P}_{0,j}$, with $P_{0,j} = n_j/n$, where n_j is the number of times that GS is found for the j -th sample in n independent runs. In the following, we estimate the error associated to P_0 .

We begin by considering the mean number of times that GS is reached for the j -th sample in n independent runs,

$$\bar{n}_j = \sum_{n_j=0}^n n_j \binom{n}{n_j} \mathcal{P}_{0,j}^{n_j} (1 - \mathcal{P}_{0,j})^{n-n_j} = n\mathcal{P}_{0,j}. \quad (\text{A.3})$$

In addition, the variance is

$$V(n_j) = \overline{(n_j - \bar{n}_j)^2} = n\mathcal{P}_{0,j}(1 - \mathcal{P}_{0,j}). \quad (\text{A.4})$$

Now, the error associated to P_0 can be estimated by calculating the variance of Eq. (A.2),

$$V(P_0) = E [(P_0 - E[P_0])^2], \quad (\text{A.5})$$

where the expected value of any quantity x is obtained as $E[x] = \langle \bar{x} \rangle$. The Eq. (A.5) can be rewritten as

$$\begin{aligned} V(P_0) &= E \left[\left(\frac{1}{N_S n} \sum_{j=1}^{N_S} n_j - \frac{1}{N_S} \sum_{j=1}^{N_S} \mathcal{P}_0 \right)^2 \right] \\ &= E \left[\left(\frac{1}{N_S n} \sum_{j=1}^{N_S} n_j - \frac{1}{N_S n} \sum_{j=1}^{N_S} n\mathcal{P}_{0,j} + \frac{1}{N_S} \sum_{j=1}^{N_S} \mathcal{P}_{0,j} - \frac{1}{N_S} \sum_{j=1}^{N_S} \mathcal{P}_0 \right)^2 \right] \\ &= \frac{1}{(N_S n)^2} \sum_{j=1}^{N_S} E [(n_j - n\mathcal{P}_{0,j})^2] + \frac{1}{(N_S)^2} \sum_{j=1}^{N_S} E [(\mathcal{P}_{0,j} - \mathcal{P}_0)^2] + \\ &+ \frac{1}{(N_S)^2 n} \sum_{j>k} E [n_j - n\mathcal{P}_{0,j}] E [\mathcal{P}_{0,k} - \mathcal{P}_0]. \end{aligned} \quad (\text{A.6})$$

As the last term disappears, we obtain

$$\begin{aligned}
 V(P_0) &= \frac{1}{(N_S n)^2} \sum_{j=1}^{N_S} \langle n \mathcal{P}_{0,j} (1 - \mathcal{P}_{0,j}) \rangle + \frac{\langle (\mathcal{P}_{0,j} - P_0)^2 \rangle}{N_S} \\
 &= \frac{\langle \mathcal{P}_{0,j} (1 - \mathcal{P}_{0,j}) \rangle}{N_S n} + \frac{\langle \mathcal{P}_{0,j}^2 \rangle - \langle \mathcal{P}_{0,j} \rangle^2}{N_S} \\
 &= \frac{\langle \mathcal{P}_{0,j} \rangle - \langle \mathcal{P}_{0,j}^2 \rangle}{N_S n} + \frac{\langle \mathcal{P}_{0,j}^2 \rangle - \langle \mathcal{P}_{0,j} \rangle^2}{N_S}.
 \end{aligned} \tag{A.7}$$

Then, the error associated to P_0 is

$$\sqrt{V(P_0)} = \sqrt{\frac{\langle \mathcal{P}_{0,j} \rangle - \langle \mathcal{P}_{0,j}^2 \rangle}{N_S n} + \frac{\langle \mathcal{P}_{0,j}^2 \rangle - \langle \mathcal{P}_{0,j} \rangle^2}{N_S}}. \tag{A.8}$$

Note that it is not necessary to consider many runs for sample: the error becomes small if many samples are considered and only one run is carried out in each one of them. Considering that $n = 1$ and $P_0 \approx \langle \mathcal{P}_{0,j} \rangle$, we approach the error of P_0 by

$$\sqrt{V(P_0)} \approx \sqrt{\frac{P_0(1 - P_0)}{N_S}}. \tag{A.9}$$

Appendix B. Tables

Parameters used in the simulation and GS energy per spin for each lattice size.

Table B1. Simulation parameters and GS energy per spin for the 2D EAB model.

L	u_L	N_S	t	P_0
3	-1.2530(2)	2×10^6	10^2	> 0.999
4	-1.3114(2)	10^6	3×10^2	> 0.999
5	-1.3497(2)	5×10^5	10^3	> 0.999
6	-1.3661(2)	2.5×10^5	3×10^3	> 0.999
7	-1.3764(2)	10^5	7×10^3	> 0.999
8	-1.3820(3)	5×10^4	1.6×10^4	> 0.999
9	-1.3854(5)	10^4	10^4	> 0.999
10	-1.3893(5)	10^4	10^4	> 0.999
12	-1.3932(4)	10^4	10^4	> 0.999
14	-1.3955(3)	10^4	10^4	> 0.999
16	-1.3973(3)	10^4	2×10^4	0.996
18	-1.3974(3)	6×10^3	4.5×10^4	0.996
20	-1.3985(4)	3×10^3	10^5	0.996
22	-1.3981(5)	2×10^3	2.5×10^5	0.996
24	-1.3994(6)	10^3	5.5×10^5	0.996
26	-1.3992(12)	2×10^2	1.2×10^6	0.996
28	-1.4001(15)	10^2	2.5×10^6	0.996
30	-1.3993(17)	10^2	5×10^6	0.996

Table B2. Simulation parameters and GS energy per spin for the 2D EAG model.

L	u_L	N_S	t	P_0
3	-1.2074(2)	2×10^6	10^2	> 0.9999
4	-1.2603(2)	10^6	3×10^2	> 0.999
5	-1.2826(3)	5×10^5	10^3	> 0.999
6	-1.2936(3)	2.5×10^5	3×10^3	> 0.999
7	-1.3000(3)	10^5	7×10^3	> 0.999
8	-1.3027(4)	5×10^4	10^4	> 0.999
9	-1.3070(8)	10^4	10^4	> 0.999
10	-1.3072(7)	10^4	10^4	0.998
12	-1.3103(6)	10^4	4×10^4	0.998
14	-1.3119(7)	5×10^3	1.5×10^5	0.998
16	-1.3119(8)	3×10^3	5.3×10^5	0.998
18	-1.3154(13)	10^3	1.7×10^6	0.998
20	-1.3127(12)	10^3	2×10^6	0.99
22	-1.3144(22)	2×10^2	2.7×10^6	0.97
24	-1.3130(23)	2×10^2	7.3×10^6	0.97
26	-1.3146(26)	10^2	8.3×10^6	0.9

Table B3. Simulation parameters and GS energy per spin for the 3D EAB model.

L	u_L	N_S	t	P_0
3	-1.6717(1)	10^6	10^2	> 0.999
4	-1.7375(1)	5×10^5	5×10^2	> 0.999
5	-1.7611(1)	10^5	2×10^3	> 0.999
6	-1.7714(3)	10^4	2×10^4	> 0.999
7	-1.7772(3)	6×10^3	2×10^5	> 0.999
8	-1.7800(3)	4×10^3	7×10^5	0.997
9	-1.7824(3)	2×10^3	1.2×10^6	0.99
10	-1.7830(3)	2×10^3	2×10^6	0.97
12	-1.7849(8)	10^2	10^7	0.93
14	-1.7858(7)	10^2	1.6×10^7	0.73

Table B4. Simulation parameters and GS energy per spin for the 3D EAG model.

L	u_L	N_S	t	P_0
3	-1.6204(2)	5×10^5	3×10^2	> 0.999
4	-1.6660(2)	2×10^5	1.5×10^3	> 0.999
5	-1.6824(3)	6×10^4	10^4	> 0.999
6	-1.6891(4)	2×10^4	5×10^4	> 0.999
7	-1.6937(8)	3×10^3	5×10^5	> 0.999
8	-1.6955(6)	3×10^3	10^6	0.997
9	-1.6966(7)	2×10^3	1.3×10^6	0.98
10	-1.6981(7)	1.3×10^3	1.6×10^6	0.90
11	-1.6982(8)	826	4.1×10^6	0.80

References

- [1] Barahona F, 1982 *J. Phys. A* **15** 3241
- [2] Holland J H, 1975 *Adaptation in Natural and Artificial Systems* (The University of Michigan Press, Ann Arbor).
- [3] Hartmann A K and Rieger H, editors, 2001 *Optimization Algorithms in Physics* (Wiley-VCH, Berlin)
- [4] Hartmann A K and Rieger H, editors, 2004 *New Optimization Algorithms in Physics* (Wiley-VCH, Berlin)
- [5] Pál K F, 1995 *Biol. Cybern.* **73** 335
- [6] Pál K F, 1996 *Physica A* **223** 283
- [7] Hartmann A K, 1996 *Physica A* **224** 480
- [8] Hartmann A K, 1997 *Europhys. Lett.* **40** 429
- [9] Houdayer J and Martin O C, 2001 *Phys. Rev. E* **64** 056704
- [10] Kirkpatrick S, Gelatt C D and Vecchi M P, 1983 *Science* **220** 671
- [11] Berg B A, Hansman U E and Celik T, 1994 *Phys. Rev. B* **50** 16444
- [12] Hukushima K and Nemoto K, 1996 *J. Phys. Soc. Japan* **65** 1604
- [13] Moreno J L, Katzgraber H G and Hartmann A K, 2003 *Int. J. Mod. Phys. C* **14** 285
- [14] Romá F, Risau-Gusman S, Ramirez-Pastor A J, Nieto F and Vogel E E, 2007 *Phys. Rev. B* **75**

020402(R)

- [15] Risau-Gusman S and Romá F, 2008 *Phys. Rev. B* **77** 134435
- [16] Edwards S F and Anderson P W, 1975 *J. Phys. F* **5** 965
- [17] Metropolis N, Rosenbluth A W, Rosenbluth N M, Teller A H and Teller E, 1953 *J. Chem. Phys.* **21** 1087
- [18] De Simone C, Diehl M, Jünger M, Mutzel P, Reinelt G and Rinaldi G, 1995 *J. Stat. Phys.* **80** 487; 1996 *J. Stat. Phys.* **84** 1363
- [19] We have used the spin-glass ground-state server of the University of Cologne where a branch-and-cut algorithm is available online, http://www.informatik.uni-koeln.de/ls_juenger/index.html
- [20] Binder K and Young A P, 1986 *Rev. Mod. Phys.* **58** 801
- [21] Pál K F, 1996 *Physica A* **233** 60
- [22] Romá F, Nieto F, Vogel E E and Ramirez-Pastor A J, 2004 *J. Stat. Phys.* **114** 1325
- [23] Katzgraber H G, Körner M and Young A P, 2006 *Phys. Rev. B* **73** 224432
- [24] Palmer R G and Adler J, 1999 *Int. J. Mod. Phys. C* **10** 667
- [25] Campbell I A, Hartmann A K and Katzgraber H G, 2004 *Phys. Rev. B* **70** 054429
- [26] Li S P, 2002 *Int. J. Mod. Phys. C* **13** 1365
- [27] Palassini M, Liers F, Jünger M and Young A P, 2003 *Phys. Rev. B* **68** 064413
- [28] Palassini M and Young A P, 1999 *Phys. Rev. Lett.* **83** 5126
- [29] Liers F and Jünger M, 2000 *Int. J. Mod. Phys. C* **11** 589